Front. Optoelectron. 2021, 14(3): 321–328
https://doi.org/10.1007/s12200-020-0978-2

RESEARCH ARTICLE

Identification of Graves' ophthalmology by laser-induced breakdown spectroscopy combined with machine learning method

Jingjing LI[1], Feng CHEN[1], Guangqian HUANG[2], Siyu ZHANG[1], Weiliang WANG[1], Yun TANG[1], Yanwu CHU[1], Jian YAO[3], Lianbo GUO (✉)[1], Fagang JIANG (✉)[2]

1 Wuhan National Laboratory for Optoelectronics, Huazhong University of Science and Technology, Wuhan 430074, China
2 Department of Ophthalmology, Union Hospital, Tongji Medical College, Huazhong University of Science and Technology, Wuhan 430022, China
3 School of Remote Sensing and Information Engineering, Wuhan University, Wuhan 430079, China

Abstract Diagnosis of the Graves' ophthalmology remains a significant challenge. We identified between Graves' ophthalmology tissues and healthy controls by using laser-induced breakdown spectroscopy (LIBS) combined with machine learning method. In this work, the paraffin-embedded samples of the Graves' ophthalmology were prepared for LIBS spectra acquisition. The metallic elements (Na, K, Al, Ca), non-metallic element (O) and molecular bands ((C-N), (C-O)) were selected for diagnosing Graves' ophthalmology. The selected spectral lines were inputted into the supervised classification methods including linear discriminant analysis (LDA), support vector machine (SVM), *k*-nearest neighbor (*k*NN), and generalized regression neural network (GRNN), respectively. The results showed that the predicted accuracy rates of LDA, SVM, *k*NN, GRNN were 76.33%, 96.28%, 96.56%, and 96.33%, respectively. The sensitivity of four models were 75.89%, 93.78%, 96.78%, and 96.67%, respectively. The specificity of four models were 76.78%, 98.78%, 96.33%, and 96.00%, respectively. This demonstrated that LIBS assisted with a nonlinear model can be used to identify Graves' ophthalmopathy with a higher rate of accuracy. The *k*NN had the best performance by comparing the three nonlinear models. Therefore, LIBS combined with machine learning method can be an effective way to discriminate Graves' ophthalmology.

Keywords Graves' ophthalmology, laser-induced breakdown spectroscopy (LIBS), linear discriminant analysis (LDA), support vector machine (SVM), *k*-nearest neighbor (*k*NN), generalized regression neural network (GRNN)

Received November 14, 2019; accepted January 4, 2020

E-mails: lbguo@hust.edu.cn, fgjiang@hotmail.com

1 Introduction

1.1 Background introduction

Graves' ophthalmopathy, also called thyroid-associated ophthalmopathy (TAO), is an eyelid disease associated with thyroid dysfunction and immune system disorder [1]. Graves' ophthalmopathy extensively affects the soft tissue of the eyelids, which can also lead to eyeball protrusion, eye movement disorder, optic nerve damage, reduced vision, and even blindness. The pathogenesis and diagnosis of Graves' ophthalmopathy have always been the research hotspot. Computed tomography (CT), magnetic resonance imaging (MRI), ultrasound (US) and related laboratory tests can be used for a screening check for thyroid dysfunction. However, some patients who had thyroid-associated ophthalmopathy did not show abnormalities in the thyroid screening test [2]. Cakir reported one case of TAO, no thyroid-related autoantibodies were detected in the blood and thyroid function was also normal [3]. No single clinical or laboratory examination is the gold standard for diagnosing thyroid eye disease for now [4]. To overcome this problem, a more stable and accurate diagnosis method is needed.

Laser-induced breakdown spectroscopy (LIBS) is an atomic and ionic emission spectroscopy technique [5]. LIBS has been widely used in meat species identification, wood species classification, soil samples analysis, oil detection, red wine classification, and material analysis and other fields [6–13], etc. In recent ten years, many

researchers have explored the application of LIBS in the biomedical field. Chen et al. diagnosed human malignancies such as lymphoma and multiple myeloma (MM) using LIBS in combination with chemometric method [14]. Ghasemi et al. used LIBS for the diagnosis of several malignant tissue samples including breast, colon, Larynx, and tongue [15]. Gaudiuso et al. diagnosed melanoma using LIBS combined with linear discriminant analysis (LDA), fisher discriminant analysis (FDA), support vector machines (SVM) and gradient boosting [16]. Chu et al. discriminated nasopharyngeal carcinoma serum using LIBS combined with extreme learning machine (ELM) and random forest (RF) [17]. To our best knowledge, no studies have been reported about identifying Graves' ophthalmology by using LIBS. Moreover, LIBS combined with generalized regression neural network (GRNN) algorithm for solving classification problems has not been investigated.

In this study, we identified between TAO paraffin embedding samples and healthy controls using LIBS combined with the LDA, SVM, *k*-nearest neighbor (*k*NN), and GRNN, respectively. We first realized the identification of Graves' ophthalmology by using LIBS combined with machine learning method, and first applied the GRNN algorithm to classify biomedical tissues combined with LIBS. The spectral lines were used as the input of classifications. The average accuracy rate, sensitivity, specificity, area under the curve (AUC), and coefficient of variation (CV) were used to evaluate the identification performance of the model.

1.2 Algorithm introduction

LDA is a classic linear supervised learning method, and it was first proposed by Fisher in 1936 on the second classification problem, also known as Fisher linear discriminant [18]. It is still one of the most widely adopted and extremely effective methods in the application of dimension reduction and pattern classification [19,20]. Compared with the neural network method, LDA does not need to adjust parameters, so there is no need such as learning parameters, optimization weights, and selection of neuron activation functions. And it is not sensitive to normalization or randomization of patterns, and this is more prominent among the various algorithms based on gradient descent.

SVM is a generalized linear classifier that classifies data in a supervised manner, it can be nonlinearly classified by using the kernel method, which is one of the common kernel learning methods [21]. SVM classification is only related to several support vectors and has strong stability and a high degree of robustness. The SVM was used for classification and regression analysis problems such as text recognition, face image recognition, plant species identification and tumor detection in machine learning and soft computing tasks [22,23].

*k*NN algorithm is one of the supervised learning methods [24]. When classifying test samples, the training samples set is first scanned, *k* samples that are most similar to the test samples set are found, and test samples are determined according to the category of *k* samples. The algorithm is not sensitive to abnormal data, simple and easy to implement. It is widely used in gender prediction, text recognition, tumor detection, and so on [25,26].

GRNN is a kind of radial basis function neural network. The network structure of GRNN has input layer, pattern layer, summation layer, and output layer [27]. It is widely used in engine performance evaluation, worsted yarn quality, and target tracking fields [28–30]. GRNN model has strong nonlinear capability and high degree of fault tolerance and robustness. As long as the training set is determined, the corresponding network structure and the connection weight between neurons are also determined accordingly. The training process of GRNN is also the process of optimizing smooth parameter σ, the parameter Spread is used to express the smooth parameter σ [31].

2 Experimental

2.1 Experimental setup

The experiment instruments are composed of a *Q*-switched Nd:YAG laser, a Czerny-Turner spectrometer, and an intensified charge-coupled device (ICCD) camera mainly. The *Q*-switched Nd:YAG laser emitted laser beam which focused on the surface of sample by a focal lens and produced the plasma. The plasma emission spectra were collected through the spectrometer and ICCD camera. The parameters about the instruments are as follows: the *Q*-switched Nd:YAG laser (wavelength: 532 nm; pulse energy: 3 mJ; repetition rate: 10 Hz; French, Quantel., Brilliant B), the Czerny-Turner spectrometer (grating: 1200 lines/mm, sparkling wavelength: 700 nm, resolution: 0.07 nm, acquisition bandwidth: 46 nm, UK, Andor Tech., Shamrock 500i) and ICCD camera (UK, Andor Tech., iStar 320T). The gate delay and the gate width of the ICCD camera were set to be 1 and 9 μs, respectively. The number of laser shots and the number of replicates were 5 and 10, respectively. The experiment instruments are shown in Fig. 1.

2.2 Sample pre-treatment

Experimental samples were collected from graves' ophthalmopathy patients and healthy controls at the Cancer Center, Union Hospital, Tongji Medical College. In total, 6 paraffin-embedded samples were donated by 3 healthy controls and 3 TAO patients. The TAO patients were diagnosed previously. It is necessary to pretreat the biological tissue samples for the analysis by LIBS. The pre-treatment steps are described below:

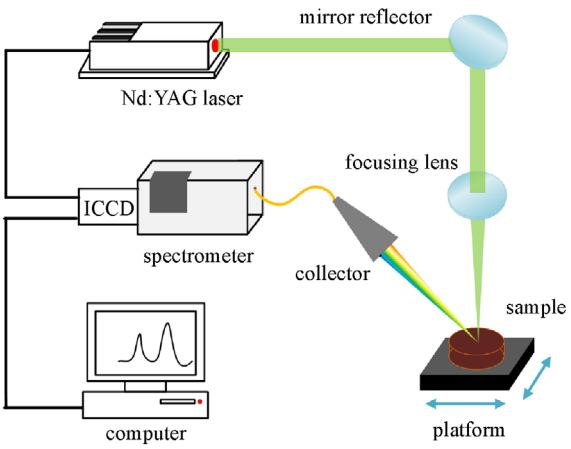

Fig. 1 Schematic diagram of the experimental setup

1) Paraffin embedding. The collected tissue was saved at −80°C first and was sent to Biossci biotechnology company Ltd (Hubei, China) to make paraffin embedding. Paraffin-embedded samples are shown in Fig. 2. Figures 2(c)–2(e) were healthy controls, and the rest was Graves' ophthalmology samples.

2) Slice. Paraffin-embedded tissue was sliced with a paraffin slicer. Each sample was sliced to 10 pieces, and every piece was 40 μm thick. Then they were placed on a glass slide, dried and stored.

The laser beam scanned a round area on the sample surface and a single spectrum was obtained by accumulating all pulses in the round area. We collected only one spectrum from one piece and 10 spectra from each sample. A total of 60 spectra were analyzed.

3 Results and discussion

3.1 Analytical line selection

The LIBS spectra from the TAO samples and healthy samples are shown in Fig. 3. We determined the elements corresponding to the observed spectral lines by comparing the National Institute of Standards and Technology (NIST) spectral database [32]. The observed elements included metallic elements (Na, K, Al, Ca), non-metallic element (O) and molecular bands ((C-N), (C-O)). The 14 spectra from one non-metallic element, two molecular bands, and four metallic elements were chosen. These 14 spectra are listed in Table 1.

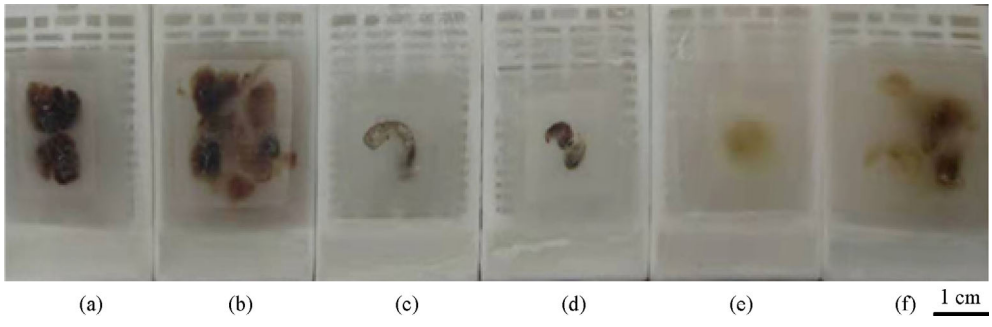

Fig. 2 Paraffin-embedded samples. (a) TAO sample; (b) TAO sample; (c) healthy sample; (d) healthy sample; (e) healthy sample; (f) TAO sample

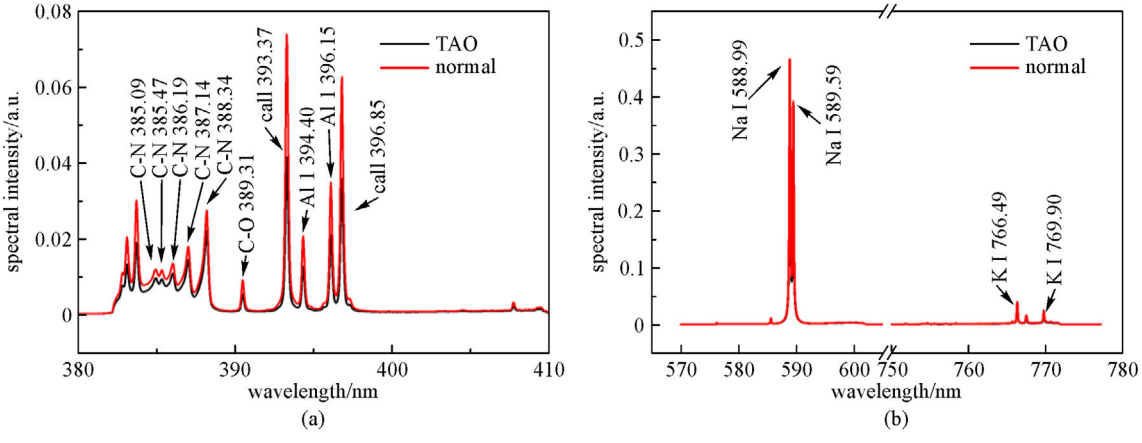

Fig. 3 LIBS spectra of two kinds of samples at different bands. (a) 380–410 nm; (b) 570–780 nm

Table 1 Analytical lines used as input variables for the classifier

	element	wavelength/nm
molecular bands	C-N	385.09, 385.47, 386.19, 387.14 388.34
	C-O	389.31
	O	383.03, 383.59
metallic elements	Na	588.99, 589.59
	K	766.49, 769.90
	Al	394.40, 396.15
	Ca	393.37, 396.85

3.2 Identification of TAO samples with the linear model

We collected ten spectra from each paraffin embedding sample. In total, 60 spectra from 3 healthy controls and 3 TAO patients are used. For each paraffin embedding sample, seven spectra were selected randomly as a training set, and the other three spectra were selected as test set. There are 42 spectra constitute to training set, and 18 spectra constitute to test set totally. The operation of random selection spectra, model training and testing were repeated 100 times. The average accuracy, precision, sensitivity, specificity, and CV were used to evaluate the model [33]. The identification results of the LDA model are shown in Table 2. The identification accuracy of the LDA model was 76.33%. The sensitivity, specificity, and precision were 75.89%, 76.78%, and 76.57%, respectively. The CV of the model was 0.0010.

The results showed that the LDA is not suitable for the identification of TAO samples. This is because LDA is a simple linear classifier that does not satisfy the classification of these data.

Table 2 Confusion matrix of the LDA model

predicted class	true class	
	TAO	normal
TAO	683	209
normal	217	691

3.3 Identification of TAO samples with the nonlinear model

In the SVM model, the radial basis function (RBF) kernel function and grid search for parameter optimization were used. The parameter optimization results were shown in Fig. 4. The results showed that the best log2*g* and log2*c* were 6 and –1, respectively. The average accuracy rate of SVM model was 96.28%. The identification results of the SVM model are shown in Table 3. The sensitivity, specificity, and precision of the SVM model were 93.78%, 98.78%, and 98.71%, respectively. The CV of the SVM model was 0.0499.

*k*NN model only has one parameter *k* that can be adjusted, and the parameter optimization result of *k* is shown in Fig. 5. When the *k*-value was 3, the *k*NN model had the best accuracy rate 96.56% and the lowest CV 0.0373. This means the model is efficient and stable. The identification results of the *k*NN model are shown in Table 4. The sensitivity, specificity, and precision of the *k*NN model were 96.78%, 96.33%, and 96.35%, respectively.

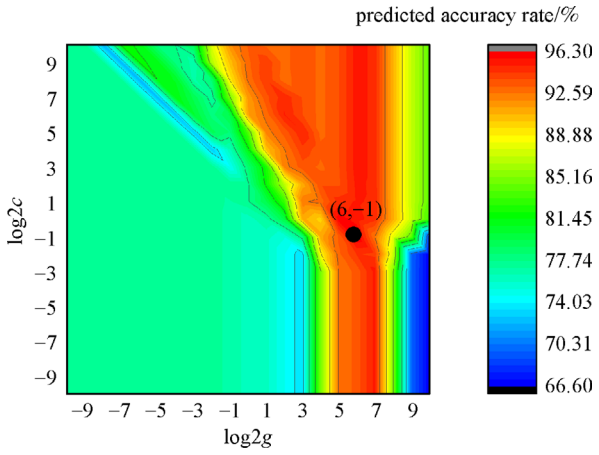

Fig. 4 Parameter optimization process of the SVM model

Table 3 Confusion matrix of the SVM model

predicted class	true class	
	TAO	normal
TAO	844	11
normal	56	889

The parameter optimization result of the Spread-value about GRNN is shown in Fig. 6. The Spread-value was from 0.01 to 0.20 and interval increased by 0.01. When the Spread-values were 0.01, 0.02, 0.03, and 0.04, the best accuracy rate was 96.33%, respectively, while the CV was 0.0378, respectively. The Spread-value reflects the approx-

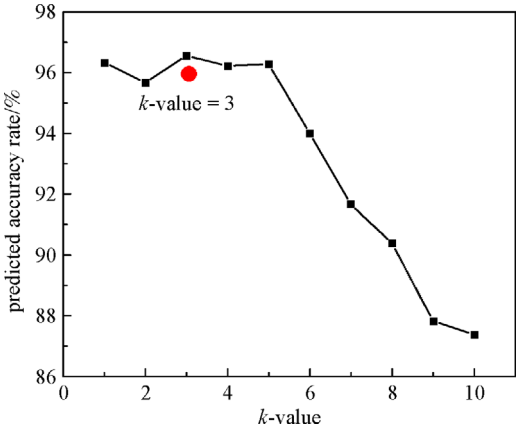

Fig. 5 Parameter optimization process of the *k*NN model

imation ability of the neutral network to the sample data. The larger Spread-value, the smoother approximation process can be acquired. To avoid overfitting, we chose 0.04 as the best Spread-value. The identification results of the GRNN model are shown in Table 5. The sensitivity, specificity, and precision of the GRNN model were 96.67%, 96.00%, and 96.03%, respectively.

Then we compared the three nonlinear models using receiver operating characteristic (ROC) curve, and area under the curve (AUC) to evaluate the quality of the models. The ROC curves of the three models are shown in Fig. 7. The AUC of the SVM, *k*NN, and GRNN models were 0.9791, 0.9695, and 0.9665, respectively. The AUC, sensitivity, and specificity of the three models are listed in Table 6.

4 Conclusions

In summary, a new approach of diagnosing Graves' ophthalmology was proposed based on LIBS combined with machine learning method. One linear model (LDA) and three nonlinear models (SVM, *k*NN, GRNN) were compared in this article. The results showed that the average accuracy rate of LDA was only 76.33%, the average accuracy rate of SVM, *k*NN and GRNN were 96.28%, 96.56%, and 96.33%, respectively, so the *k*NN model had the best average accuracy rate. The sensitivity of the three nonlinear models were 93.78%, 96.78%, and 96.67%, respectively and the specificity of the three nonlinear models were 98.78%, 96.33%, and 96.00%, respectively. The *k*NN model had the best sensitivity, but its specificity was slightly worse than the SVM model's. Sensitivity means the percentage of positive samples detected, whereas specificity means the percentage of negative samples detected. For the detection of biomedical samples, we pay more attention to the detection rate of positive samples. Therefore, we can conclude that *k*NN is slightly better than SVM. Moreover, the various evaluation indicators of the *k*NN model were slightly better than those of the GRNN model. Among the four models, the *k*NN model had the best performance. Therefore, LIBS combined with machine learning method can be an effective way to distinguish Graves' ophthalmology.

Table 4 Confusion matrix of the *k*NN model

predicted class	true class	
	TAO	normal
TAO	871	33
normal	29	867

Table 5 Confusion matrix of the GRNN model

predicted class	true class	
	TAO	normal
TAO	870	36
normal	30	864

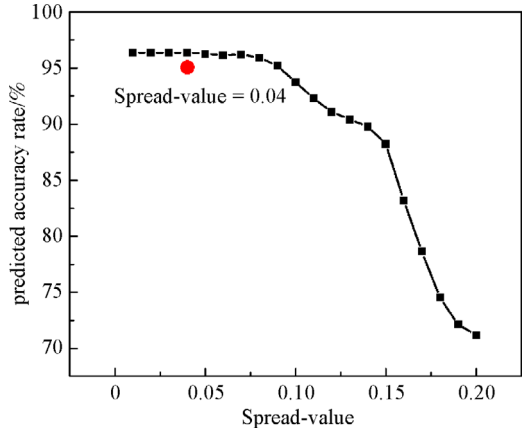

Fig. 6 Parameter optimization process of the GRNN model

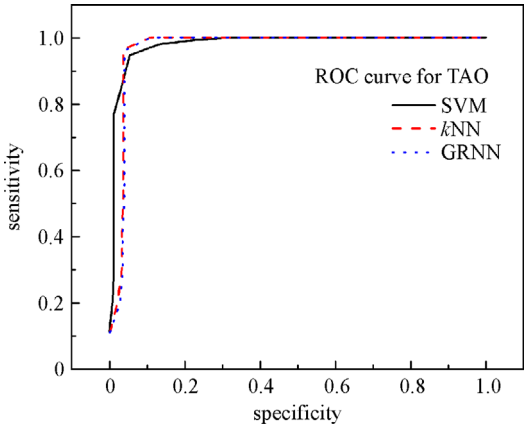

Fig. 7 ROC curves obtained with three nonlinear identification model

Table 6 Indicators of the nonlinear identification models

	AUC			sensitivity			specificity		
	SVM	*k*NN	GRNN	SVM	*k*NN	GRNN	SVM	*k*NN	GRNN
test set	0.9791	0.9695	0.9665	0.9378	0.9678	0.9667	0.9878	0.9633	0.9600
training set	1	0.9699	1	1	1	1	1	0.9671	1

Acknowledgements This work was supported by the National Natural Science Foundation of China (Grant No. 61575073). The authors would also like to acknowledge valuable discussions with the master student Haohao Cui.

Disclosures The authors declare that there are no conflicts of interest related to this article.

References

1. Bahn R S. Graves' ophthalmopathy. The New England Journal of Medicine, 2010, 362(8): 726–738
2. Phelps P O, Williams K. Thyroid eye disease for the primary care physician. Disease-a-Month, 2014, 60(6): 292–298
3. Cakir M. Euthyroid Graves' ophthalmopathy with negative autoantibodies. Journal of the National Medical Association, 2005, 97(11): 1547–1549
4. Heufelder A E. Pathogenesis of ophthalmopathy in autoimmune thyroid disease. Reviews in Endocrine & Metabolic Disorders, 2000, 1(1–2): 87–95
5. Guo L, Li X, Xiong W, Zeng X, Lu Y. Recent technological progress in Asia from the first Asian Symposium on Laser-induced Breakdown Spectroscopy. Frontiers of Physics, 2016, 11(6): 115208
6. Leandro J G R, Gonzaga F B, de Figueiredo Latorraca J V. Discrimination of wood species using laser-induced breakdown spectroscopy and near-infrared reflectance spectroscopy. Wood Science and Technology, 2019, 53(5): 1079–1091
7. Akhtar M, Jabbar A, Ahmed N, Mahmood S, Umar Z A, Ahmed R, Baig M A. Analysis of lead and copper in soil samples by laser-induced breakdown spectroscopy under external magnetic field. Applied Physics B, Lasers and Optics, 2019, 125(6): 110
8. Trichard F, Forquet V, Gilon N, Lienemann C, Baco-Antoniali F. Detection and quantification of sulfur in oil products by laser-induced breakdown spectroscopy for on-line analysis. Spectrochimica Acta Part B, Atomic Spectroscopy, 2016, 118: 72–80
9. Moncayo S, Rosales J D, Izquierdo-Hornillos R, Anzano J, Caceres J O. Classification of red wine based on its protected designation of origin (PDO) using Laser-induced Breakdown Spectroscopy (LIBS). Talanta, 2016, 158: 185–191
10. Jochum T, Günther J U, Bohling C. Material Analysis in Fast Industrial Processes by LIBS: Technical and analytical solutions for inline process monitoring. Photonics Views, 2019, 16(1): 56–59
11. Guo L B, Zhu Z H, Li J M, Tang Y, Tang S S, Hao Z Q, Li X Y, Lu Y F, Zeng X Y. Determination of boron with molecular emission using laser-induced breakdown spectroscopy combined with laser-induced radical fluorescence. Optics Express, 2018, 26(3): 2634–2642
12. Yuan R, Tang Y, Zhu Z, Hao Z, Li J, Yu H, Yu Y, Guo L, Zeng X, Lu Y. Accuracy improvement of quantitative analysis for major elements in laser-induced breakdown spectroscopy using single-sample calibration. Analytica Chimica Acta, 2019, 1064: 11–16
13. Chu Y W, Tang S S, Ma S X, Ma Y Y, Hao Z Q, Guo Y M, Guo L B, Lu Y F, Zeng X Y. Accuracy and stability improvement for meat species identification using multiplicative scatter correction and laser-induced breakdown spectroscopy. Optics Express, 2018, 26 (8): 10119–10127
14. Chen X, Li X, Yu X, Chen D, Liu A. Diagnosis of human malignancies using laser-induced breakdown spectroscopy in combination with chemometric methods. Spectrochimica Acta Part B, Atomic Spectroscopy, 2018, 139: 63–69
15. Ghasemi F, Parvin P, Reif J, Abachi S, Mohebbifar M R, Razzaghi M R. Laser induced breakdown spectroscopy for the diagnosis of several malignant tissue samples. Journal of Laser Applications, 2017, 29(4): 042005
16. Gaudiuso R, Ewusi-Annan E, Melikechi N, Sun X, Liu B, Campesato L F, Merghoub T. Using LIBS to diagnose melanoma in biomedical fluids deposited on solid substrates: Limits of direct spectral analysis and capability of machine learning. Spectrochimica Acta Part B, Atomic Spectroscopy, 2018, 146: 106–114
17. Chu Y, Chen T, Chen F, Tang Y, Tang S, Jin H, Guo L, Lu Y, Zeng X. Discrimination of nasopharyngeal carcinoma serum using laser-induced breakdown spectroscopy combined with an extreme learning machine and random forest method. Journal of Analytical Atomic Spectrometry, 2018, 33(12): 2083–2088
18. Fisher R A. The use of multiple measurements in taxonomic problems. Annals of Eugenics, 1936, 7(2): 179–188
19. Ghassabeh Y A, Rudzicz F, Moghaddam H A. Fast incremental LDA feature extraction. Pattern Recognition, 2015, 48(6): 1999–2012
20. Zhang Y K, Liu C Q. A novel face recognition method based on linear discriminant analysis. Journal Infrared Millimeter and Waves, 2003, 22(5): 327–330
21. Boser B E, Guyon I M, Vapnik V N. A training algorithm for optimal margin classifiers. In: Proceedings of the 5th annual workshop on Computational learning theory. New York: ACM, 1992, 144–152
22. Goyal N, Gupta K, Kumar N. Multiclass twin support vector machine for plant species identification. Multimedia Tools and Applications, 2019, 78: 27785–27808
23. Chu Y W, Chen F, Tang Y, Chen T, Yu Y X, Jin H L, Guo L B, Lu Y F, Zeng X Y. Diagnosis of nasopharyngeal carcinoma from serum samples using hyperspectral imaging combined with a chemometric method. Optics Express, 2018, 26(22): 28661–28671
24. Kataria A, Singh M D. A review of data classification using *k*-nearest neighbour algorithm. International Journal of Emerging Technology and Advanced Engineering, 2013, 3: 354–360
25. Dogan O, Oztaysi B. Genders prediction from indoor customer paths by Levenshtein-based fuzzy *k*NN. Expert Systems with Applications, 2019, 136: 42–49
26. Jiang S, Pang G, Wu M, Kuang L. An improved *k*-nearest-neighbor algorithm for text categorization. Expert Systems with Applications, 2012, 39(1): 1503–1509
27. Celikoglu H B. Application of radial basis function and generalized regression neural networks in non-linear utility function specification for travel mode choice modelling. Mathematical and Computer Modelling, 2006, 44(7-8): 640–658
28. Han S, Huang L, Zhou Y, Liu Z. Mixed chaotic FOA with GRNN to construction of a mutual fund forecasting model. Cognitive Systems Research, 2018, 52: 380–386
29. Hu Z, Zhao Q, Wang J. The prediction model of worsted yarn quality based on CNN–GRNN neural network. Neural Computing & Applications, 2019, 31(9): 4551–4562

30. Bendu H, Deepak B, Murugan S. Application of GRNN for the prediction of performance and exhaust emissions in HCCI engine using ethanol. Energy Conversion and Management, 2016, 122: 165–173
31. Zhang Y, Niu J, Na S.A novel nonlinear function fitting model based on FOA and GRNN. Mathematical Problems in Engineering, 2019, 2019: 2697317
32. NIST. NIST Atomic Spectra Database. 2014
33. Zhu W, Zeng N, Wang N. Sensitivity. Specificity, Accuracy, Associated Confidence Interval and ROC Analysis with Practical SAS® Implementations, 2010

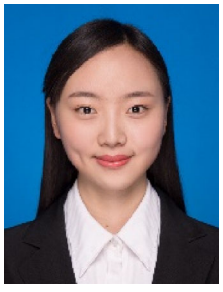

Jingjing Li received the B.S. degree in Biomedical Engineering from the School of Electrical Engineering at Zhengzhou University of China in 2017. She is now a master student at the Wuhan National Laboratory for Optoelectronics, Huazhong University of Science and Technology, China. Her research interest is application of laser technology in biomedical field.

Feng Chen received the B.S. degree in Applied Physics from the School of Space Science and Physics at Shandong University of China in 2017. He is now a Ph.D. student at the Wuhan National Laboratory for Optoelectronics, Huazhong University of Science and Technology, China. His research interest is in laser-induced breakdown spectroscopy.

Guangqian Huang graduated from Tongji Medical College of Huazhong University of Science and Technology with an eight-year degree in clinical medicine and a doctor of clinical medicine (ophthalmology). Since August 2019, he has worked as a resident in the ophthalmology department of the Second Affiliated Hospital of Fujian Medical University. The main direction is orbital diseases, including thyroid-related eye diseases, orbital tumors, and orbital fractures.

Siyu Zhang received the B.S. degree in Materials Science and Engineering at Northeast Forestry University of China in 2018. She is now a master student at the Wuhan National Laboratory for Optoelectronics, Huazhong University of Science and Technology, China. Her research interest is laser-induced breakdown spectroscopy.

Weiliang Wang received the B.S. degree in Electrical Engineering and Automation from the School of Electrical and Automation Engineering at Nanjing Normal University (NNU) of China in 2019. He is currently working toward the M.S. degree in Electronic Science and Technology in Huazhong University of Science and Technology, China. His research work focuses on the Laser-induced breakdown spectroscopy (LIBS).

Yun Tang is currently a lecturer at the School of Physics and Electronic Science, Hunan University of Science and Technology (HNUST), Xiangtan, China. She received the Ph.D. degree in Electronic Science and Technology from Wuhan National Laboratory for Optoelectronics (WNLO) at Huazhong University of Science and Technology (HUST) of China in 2019. She has published more than 20 papers in the fields of laser-induced breakdown spectroscopy.

Yanwu Chu received the B.S. degree in Optical Engineering at China Three Gorges University in 2016. He is now a doctoral student at the Wuhan National Laboratory for Optoelectronics, Huazhong University of Science and Technology, China. His research interest is laser-induced breakdown spectroscopy and biophotonics.

Prof. **Jian Yao** is a Hubei "Chutian Scholar" Distinguished Professor with the School of Remote Sensing and Information Engineering and the Director of the Computer Vision and Remote Sensing (CVRS) Lab and the 3D Big Data and AI Innovation Research Centre, Wuhan University, China. He worked as a Professor with the Shenzhen Institutes of Advanced Technology (SIAT),Chinese Academy of Sciences, China from 2011 to 2012. He has published over 120 articles in international journals and proceedings of major conferences and is the inventor of over 80 patents. His current research interests mainly include computer vision, image processing, machine learning, deep learning, LiDAR data processing, robotics, etc.

Prof. **Lianbo Guo** is a doctoral supervisor of Wuhan National Laboratory for Optoelectronics (WNLO), and graduate supervisor of China-EU Institute for Clean and Renewable Energy at Huazhong University of Science and Technology (HUST), China. He had been a visiting scholar in the Department of Electrical Engineering in University of Nebraska Lincoln from 2010 to 2012 and received his Ph.D. degree in Electronic Science and Technology from WNLO in 2012. Dr. Guo is a special expert of Wuhan city "3551 talents plan" and a member of the academic committee of laser-induced breakdown spectroscopy of Chinese Society of Optical Engineering, Fellow of OSA and SPIE. He is a reviewer of many international renowned journals, such as *Applied physics Letters*, *Optics Express* and *Optics Letters*.

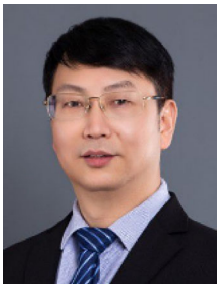

Prof. **Fagang Jiang** is chief physician of Department of Ophthalmology in Union Hospital of Tongji Medical College at Huazhong University of Science and Technology (HUST). He received the Ph.D. degree from Tongji Medical College at HUST from 1992 to 1995 and had been a visiting doctor in University of Saarland, Germany from 2000 to 2001. His research interests are mainly in orbital diseases, thyroid-associated ophthalmopathy, nerve-ophthalmology, and ocular trauma.